

# Deflagration to Detonation Transition Processes by Turbulence-Generating Obstacles in Pulse Detonation Engines

Seong-Young Lee,\* Jonathan Watts,<sup>†</sup> Silvano Saretto,<sup>‡</sup> Sibtos Pal,<sup>§</sup> Chris Conrad,<sup>†</sup> Roger Woodward,\* and Robert Santoro<sup>¶</sup>  
*The Pennsylvania State University, University Park, Pennsylvania 16802*

The results from a series of detonation experiments conducted to characterize the deflagration-to-detonation transition (DDT) process for ethylene-air mixtures in a 44-mm-square, 1.65-m-long tube are described. Experiments were conducted for both single-shot detonations involving quiescent mixtures as well as multicycle detonations involving dynamic fill. For the experiments, high-frequency pressure and flame emission measurements were made to obtain the compression wave and flame speeds, respectively. In addition, schlieren and hydroxyl-radical/planar-laser-induced-fluorescence (OH-PLIF) imaging were applied to investigate the interactions between the shock-wave and combustion phenomena during both deflagration and detonation. For ethylene-air mixtures, strategically placed obstacles were necessary to achieve DDT. The effect of the presence of obstacles on flame acceleration was systematically investigated by changing the obstacle configuration. The parametric study of obstacle blockage ratio, spacing between obstacles, and length of the obstacle configuration indicated that for successful detonations the obstacle needs to accelerate the flame to a minimum flame speed of roughly half the Chapman–Jouguet detonation velocity. Differences in the flame and compression wave velocities demonstrated the development of a coupled feedback mechanism as the wave propagated along the tube. A series of simultaneous schlieren and OH-PLIF images showed that the obstacle plays a major role in generating small/large-scale turbulence that enhances flame acceleration. Localized explosions of pockets of unburned mixture further enhanced the shock-wave strength to continuously increase the flame speed. The results of this experimental study support the importance of obstacles as a means to enhance DDT and provide a potential solution for practical pulse-detonation-engine applications.

## Introduction

RECENT interest in pulse detonation engines (PDEs) has resulted in several experimental and theoretical studies related to realizing multicycle detonations in tubes that simulate engine operating conditions.<sup>1–5</sup> These studies make a clear case that pulse detonation engines provide the potential for higher specific impulse, reduced complexity, and lower operational costs as compared to current gas turbine technology. For airbreathing applications, hydrocarbon-air propellant combinations are being considered, which are particularly difficult to detonate within a practical length.<sup>6</sup> In addition, a key barrier to the realization of an operational PDE is achieving reliable and repeatable detonations in the shortest distance possible to minimize system weight.

Over the past several decades, researchers have employed a series of repeated obstacles along the flow path to enhance flame acceleration in order to achieve self-sustained detonations.<sup>6–12</sup> Fundamentally, obstacle-induced turbulence increases the flame burning rate by increasing the flame surface area and the transport of local mass and energy. Moreover, turbulence scales play a significant role in flame acceleration associated with burning rate. In the earlier stage of flame evolution upon mild ignition, large scales of turbulence are necessary to increase the surface area or flame folding, whereas excess flame stretching and rapid mixing of the burned gas can have an adverse effect on further flame evolution, which can cause the flame

to completely quench. Once the flame evolves into the distributed reaction zone and thus, transforms into a turbulent flame brush, finer turbulence scales are necessary to increase the flame surface area within the flame brush.<sup>7,10,11</sup> Therefore, optimizing the design of the obstacle configuration is necessary for reducing both deflagration-to-detonation transition (DDT) length and time in a practical PDE as direct detonation initiation in flight vehicles would require an impractical amount of energy.<sup>13,14</sup> In addition, Kiyanda et al.<sup>14</sup> experimentally studied detonation phenomena in a tube without internal obstacles and suggested that as long as the mixture is burned inside the tube the impulse produced by direct detonation ignition and DDT is the same. However, Cooper et al.<sup>15</sup> reported that the measured impulse with internal obstacles is reduced by an average of 25% as compared to the measured impulse for a tube without internal obstacles in their impulse measurements for various obstacle configurations. Thus, minimizing DDT length is a fundamental goal in PDE development, but must also be achieved in such a manner as not to reduce engine thrust. Additionally, if obstacles are employed they must be rugged and lightweight from an engine systems and reliability perspective.

The fast deflagration velocity generated by the turbulent flame acceleration process relies on various parameters, including the sensitivity of the mixture composition, the dimensions of the detonation tube and the size, shape and distribution of the obstacles.<sup>6,7,10,16</sup> Essentially, the flame acceleration process by either obstacle-induced flow or naturally occurring flow instabilities eventually leads to the DDT process throughout the shock-induced combustion ignition region by the positive feedback coupling mechanism between the shock and the flame. The DDT process is often followed by the formation of explosion centers from pockets of reactants, which create blast waves and the process is continuously amplified through multi-shock interactions with the flame.<sup>17–19</sup> In addition, large-scale experiments performed by Dorofeev et al.<sup>20</sup> have shown that turbulent mixing of fresh and burned gases reduces the sensitivity of the mixture composition for the onset of DDT compared to the laboratory-scale experiment. Experiments and computational investigations of the DDT process demonstrate that the explosion could occur between the leading shock and the flame shock, at the flame front, at the shock front, or at the contact discontinuity formed by the coalescence of shock waves that precede the flame.<sup>17,18</sup> It has been also

Received 1 October 2002; accepted for publication 6 May 2004. Copyright © 2004 by Robert Santoro. Published by the American Institute of Aeronautics and Astronautics, Inc., with permission. Copies of this paper may be made for personal or internal use, on condition that the copier pay the \$10.00 per-copy fee to the Copyright Clearance Center, Inc., 222 Rosewood Drive, Danvers, MA 01923; include the code 0748-4658/04 \$10.00 in correspondence with the CCC.

\*Research Associate, Department of Mechanical and Nuclear Engineering.

<sup>†</sup>Graduate Student, Department of Mechanical and Nuclear Engineering.

<sup>‡</sup>Postdoctoral Scholar, Department of Mechanical and Nuclear Engineering.

<sup>§</sup>Senior Research Associate, Department of Mechanical and Nuclear Engineering.

<sup>¶</sup>Professor, Department of Mechanical and Nuclear Engineering.

observed that DDT is generated from the explosion resulting from the reignition of partially quenched unburned mixture behind obstacles within the path of the deflagration wave.<sup>19,21</sup> Finally, with the DDT process, a detonation wave is formed as a result of coupling between the amplified compression waves and the reaction zone.

During the turbulent flame acceleration before transition to detonation, shock waves also form in the flow, which further increases the burning rate such that the energy released by chemical reactions generates weak compression waves that propagate into the reactants ahead of the flame and form the initial shock wave ahead of the reaction zone. As the flame accelerates, the product temperature increases, which results in an increase in the sonic velocity and consequently allows the acoustic waves to merge into a shock wave ahead of the flame. When the shock wave gains sufficient energy to initiate chemical reactions, shock-induced combustion occurs as the flame moves downstream. The close coupling of the energy release and the shock wave strengthens the feedback system between them, further increasing the shock-wave strength and the reaction rate, resulting in the formation of a self-sustained detonation wave.<sup>17,19</sup> Combustion rate enhancement depends on the amplitude of the shock wave and the chemical reactivity of the unburned mixture.

Although significant research has been performed in the past to understand DDT phenomena including the use of obstacles to accelerate transition, direct observation of such phenomena has seldom been attempted for multicycle operations. Previous research was performed using long tubes and mixtures of easily detonable fuels such as hydrogen or acetylene with pure oxygen, which cannot be used in a practical airbreathing PDE system.<sup>6,8,9</sup> The difficulty in sustaining a detonation depends on several parameters including tube geometry, choice of fuel and oxidizer, equivalence ratio, presence and concentration of inert gases, spark energy, initial chamber pressure and temperature, and obstacle configuration. Therefore, the optimization of the system is necessary to produce the desired detonation by considering the parameters just listed for the practical PDE.

The objective of the present study is to investigate design strategies that minimize the distance required to achieve DDT in mixtures of hydrocarbon fuel and air. An in-house developed obstacle geometry is utilized for the experiments. The obstacle size, distance between obstacles, and the length of the obstacle configuration were optimized to obtain a minimum DDT length for hydrocarbon-air combustion. In situ schlieren, planar laser-induced fluorescence (PLIF) from hydroxyl radicals (OH), and flame emission imaging diagnostics were employed to visualize the shock wave, reaction

zone, and heat release, respectively. Shock and flame speeds were measured using an array of high-frequency pressure transducers and photodiodes mounted on the tube. In this paper, experimental results are presented for both single-shot detonations in quiescent mixtures as well as multicycle detonations. The initial single-shot experiments involving quiescent mixtures were conducted as a basis for comparison with results from multicycle operation.

## Experimental Setup

The DDT experiments were carried out in a 1.65-m-long-square tube with a 44 × 44 mm cross section as shown in Fig. 1a. The cross-sectional dimensions were chosen to accommodate detonations of most hydrocarbon-air mixtures.<sup>22</sup> The detonation tube incorporated four interchangeable sections including an optically accessible section (window access on four sides). The obstacle used in this study consisted of flat plates mounted in a helical pattern as shown in Fig. 1b, similar in concept to a Shchelkin spiral.<sup>6</sup> Obstacles were mounted on four rods positioned inside the tube using T-shaped supports. The obstacle configuration was structurally robust to withstand detonation impulses, designed for ease in reconfiguration to facilitate rapid design optimization, and accessible to optical diagnostics.

Ethylene ( $C_2H_4$ ) was selected as the fuel, because of its well-documented detonation properties with air<sup>23</sup> and because it is a common decomposition component of heavy hydrocarbon species typical of liquid fuels. For the baseline single-shot detonation experiments, ethylene and air propellants at an equivalence ratio of 1.2 were used because it is relatively easy to achieve detonation combustion as a result of the propellant combination's minimal cell size. Before filling the detonation tube, the open tube end was sealed with a 2- $\mu$ m-thick Mylar film, and the tube was evacuated to 3.1 torr. The tube was then filled with the premixed fuel-air mixture to room temperature and atmospheric pressure conditions. The quiescent mixture was ignited at the closed end of the tube using a  $\sim 25$  J spark with a pulse duration of about 20  $\mu$ s. Upon reaching the tube exit, the wave broke through the Mylar film.

During multicycle experiments, the propellants were injected into the detonation tube using the impinging jet injector shown in Fig. 1c. This injector design concept is based on conventional rocket injector designs for achieving rapid mixing. The injector has 16 impinging jet elements. Each element has a central fuel hole (1.7 mm) and six angled (30 deg) oxidizer holes (2.0 mm). Impingement of the oxidizer jet on the central fuel jet ensures that a well-mixed flowfield

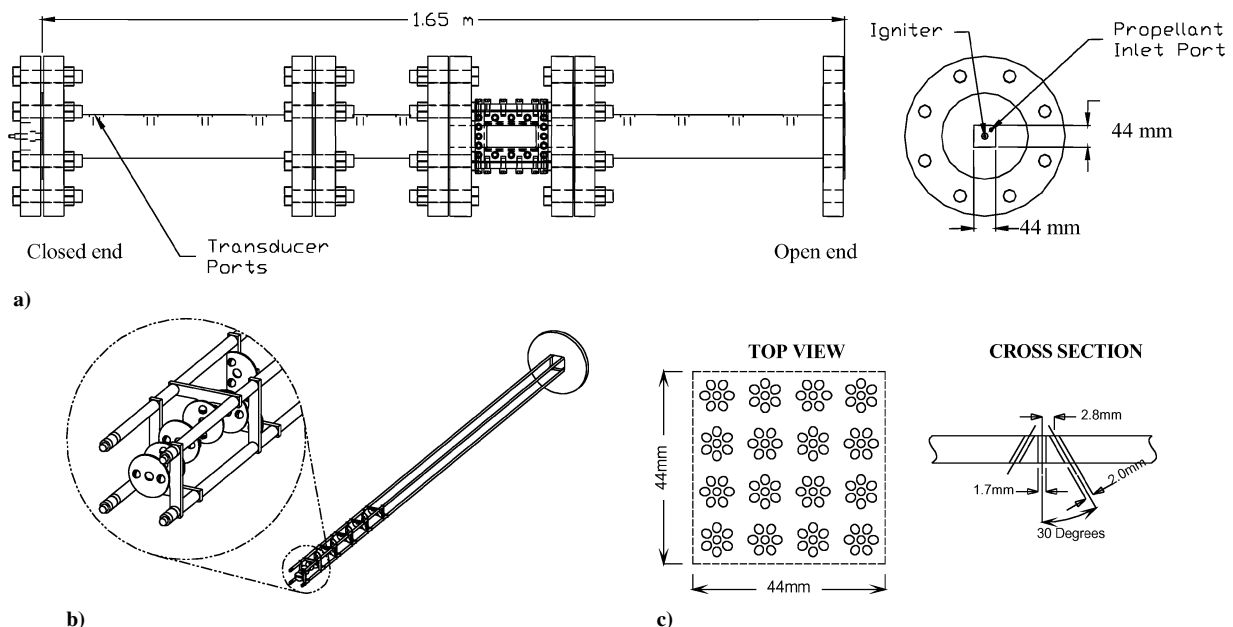


Fig. 1 Schematic of detonation tube experiment: a) optically accessible square detonation tube, b) obstacle configuration, and c) propellant injector design. The sizes of the fuel and oxidizer holes are 1.7 and 2.0 mm, respectively.

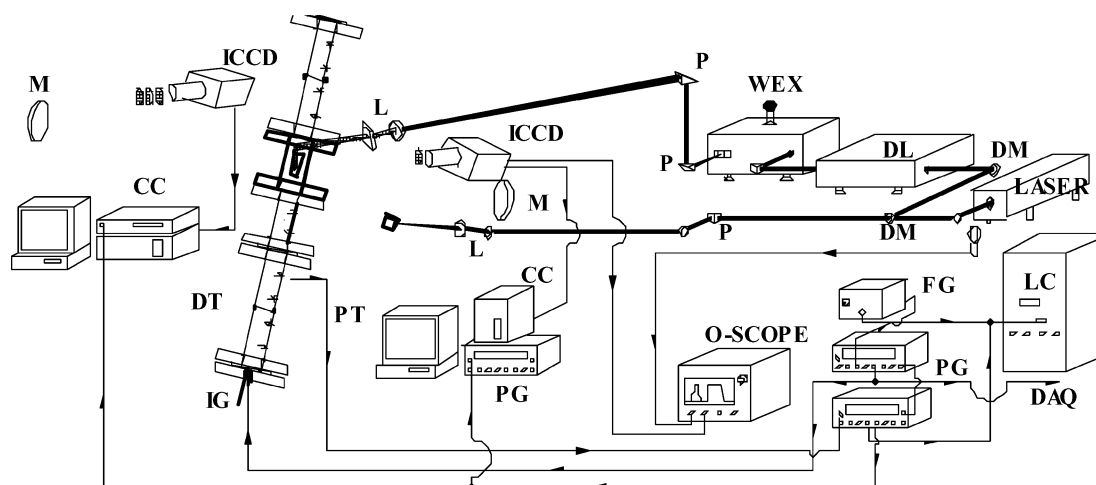


Fig. 2 Optical setup of the laser spark schlieren and OH-PLIF imaging system: CC, camera controller; DAQ, data acquisition; DL, dye laser; DM, dichroic mirror; DT, detonation tube; FG, function generator; ICCD, intensified CCD; IG, igniter; L, lens controller; LC, laser controller; M, mirror; P, prism; PG, pulse generator; PT, pressure transducer; and WEX, wavelength extender.

is achieved in a short distance from the injector face. A spark plug was mounted transverse to the axis of the tube, 22 mm from the injector face. The injector assembly adds 60 mm to the length of the detonation tube. This injector assembly was not installed on the detonation tube for the single-shot experiments. The propellant flows in multicycle operation were controlled by fast response solenoids, with opening and closing times of  $\sim 3$  ms, which were calibrated as metering orifices. Several detonations (typically  $\sim 20$ ) of ethylene and air with equivalence ratio of 1.2 at 10 Hz were generated for the multicycle experiments. For a cycle, ethylene (4.4 g/s) and air (53.3 g/s) were delivered in 70 ms through the injector resulting in a mixture bulk velocity of approximately 25 m/s. The propellant valves were then closed, and the mixture was ignited using the same  $\sim 25$  J spark as employed in the single-shot experiments. The mixture would then detonate, and the tube was allowed to aspirate back to atmospheric pressure. A small amount of buffer air (5–10 ms) injected before the propellant charge for a cycle was found to dramatically improve detonation uniformity and repeatability.

OH-PLIF and schlieren images were acquired simultaneously using the experimental apparatus shown in Fig. 2. The frequency-doubled laser beam from a Nd:YAG laser at 532 nm with nominal power of 230 mJ/pulse was split into two beam propagation paths using a dichroic mirror in order to provide the light source for the schlieren system and the UV excitation beam for OH-PLIF simultaneously.

The first beam was used to pump a dye laser, and the dye laser output was frequency doubled using a wavelength extender to obtain the 283.01-nm (vacuum) UV beam with pulse energies of approximately 6.5 mJ for excitation of the OH  $Q_1(6)$  transition. The laser sheet for the PLIF measurements was formed with a combination of a cylindrical and a spherical lens and directed into the optically accessible section from the top. The 0.4-mm-thickness sheet was positioned along the tube centerline. Window access provided a field of view of  $100 \times 44$  mm. UG11 and WG 305 Schott glass filters were placed in front of an  $f/4.5$ , 105-mm UV lens mounted on an intensified charge-coupled device (ICCD) camera. A 100-ns camera intensifier gatewidth was used to minimize interference from flame emission. When imaging the detonation region, one more UG11 glass filter was added in front of the camera to prevent ICCD saturation.

The schlieren system was set up in a standard Z arrangement. The second 532-nm beam was focused on an aluminum plate, and the resulting spark of incoherent light was used as a point light source. This light was collimated by a 1-m focal length, 146-mm-diam concave mirror and sent through the test section. The collimated light was collected by an identical mirror on the opposite side of the test section and then refocused through neutral density filters and a blue filter to reduce combustion light onto a razor blade. The razor

edge was vertically oriented to observe the density gradients of the medium along the tube axis. The density gradients were imaged through an  $f/4.5$ , 60-mm lens onto a second intensified camera with a 200-ns gatewidth.

The experiments were run remotely using an electronic pulse generator that triggered the igniter, data-acquisition system, and the propellant valves during multicycle operation. A high-frequency pressure transducer mounted on the detonation tube was used to trigger the laser and both ICCD cameras to capture the combustion event at the proper location in the tube. To monitor the combustion wave's pressure rise and flame emission, transducers were mounted along the tube, as shown in Fig. 1a. High-frequency pressure transducers were used to measure the compression wave arrival time, and fast response photodiodes were used to measure the time of arrival of the flame emission. The signals were sampled at 5 MHz using a data-acquisition system interfaced to a computer. The arrival times and transducer positions were used to calculate flame and compression wave velocities.

## Results and Discussion

### Single-Shot Results

#### Velocity Measurements

A series of systematic experiments were performed to investigate the effect of various obstacle configuration parameters on the process of transition from a low-speed flame to a fully developed detonation. This series of experiments were all performed with single-shot detonations of ethylene-air at an equivalence ratio of 1.2 at atmospheric pressure and room-temperature conditions. For reference, the Chapman–Jouguet (C-J) detonation velocity for these experimental conditions was calculated to be 1865 m/s using a chemical equilibrium code.<sup>24</sup> The C-J deflagration velocity, the so-called “choking regime,” is the maximum deflagrative burning velocity, which propagates at the sound speed of the combustion products.<sup>25–27</sup> For the current conditions, it would be about 1030 m/s based on the sound speed of the combustion products.<sup>24</sup> According to Chue et al.,<sup>27</sup> the maximum deflagrative velocity strongly depends on the energetic properties of the mixture rather than the flame structure.

The obstacle configuration parameters that were examined included the obstacle size, spacing (pitch), and the obstacle configuration length. The obstacle pitch is defined as four times the spacing between adjacent obstacles. Numerous configurations were tested, but only eight of the most representative cases will be discussed here in conjunction with detonation characteristics related to flame acceleration. The eight configurations under consideration are summarized in Fig. 3. The fraction of the tube blocked by an obstacle is called the blockage ratio (BR) and is defined as the ratio of the

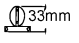
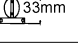
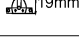
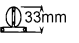
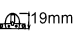
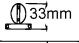
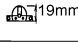
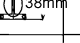
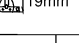
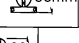
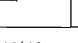
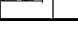
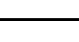
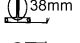
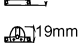
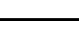
Obstacle Size and Scale		
Obstacle	Pitch	0.5 m 1 m
C1	47mm	
C2	94mm	
C3	94mm	
C4	94mm	 
C5	94mm	 
C6	94mm	 
C7	94mm	 
C8	94mm	 
		BLOCKAGE RATIO
		 0.55
		 0.41
		 0.28

Fig. 3 Obstacle configurations for DDT experiments.

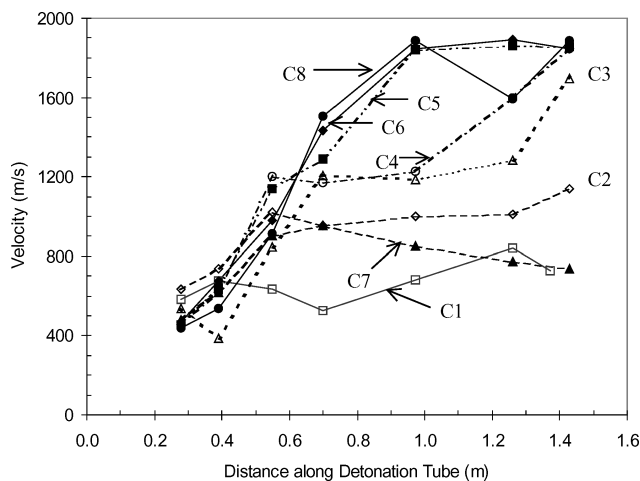


Fig. 4 Compression wave average velocities corresponding to the obstacle configurations from Fig. 3.

projected area of the obstacle to the cross-sectional area of the detonation tube. Blockage ratios of 0.55, 0.41, and 0.28 were studied.

The calculated average wave velocity between a pair of transducers is the ratio of the distance between the transducers to the difference of the wave arrival times at each location. For the current study, the error associated with the velocity measurement was found to be 8% at the detonation velocity. The average velocities for different obstacle configurations as a function of axial location are plotted in Fig. 4, which shows the influence of obstacle configuration parameters on flame acceleration. Only a series of weak pressure waves are observed at the head of the tube, which have no clear wave arrival time, and so the first two pressure transducers were not used in velocity calculations.

The results shown in Fig. 4 indicate that successful transition to detonation within the tube depends on the obstacle configuration parameters, an observation also noted in Refs. 6 and 7. Three different general velocity profiles can be classified from the results in Fig. 4: 1) failure to reach detonation velocity (configurations C1,C2,C7) in which only a fast deflagration velocity is achieved; 2) reaching C-J detonation velocity at the tube exit with some extended periods of propagation at the C-J deflagration velocity (C3,C4); and 3) achieving C-J detonation velocity at some point before the tube exit with continuous acceleration through the C-J deflagration velocity (C5,C6,C8).

The effect of the obstacle pitch on flame acceleration is demonstrated for configurations C1 and C2 where the pitch has been dou-

bled. The wave velocity profiles show similar trends in the initial stages for configurations C1 and C2, but the maximum velocity is considerably greater for configuration C2. When the obstacle pitch becomes too small, the momentum loss of driving the flow through the obstacles exceeds the benefits in flame acceleration. In both configurations C1 and C2, the obstacle configuration length is long enough for the flame velocities to reach nearly steady values as a balance is reached between the accelerating influence of the obstacle-induced turbulence and the flow momentum lost as a result of interaction with the obstacles.

The overall effect of blockage ratio on the velocity profile is observed by comparing configurations C2 and C3 where the pitch and length of the obstacle configuration are held constant, but blockage ratio is changed. The amount of flame acceleration produced depends highly on both the large- and small-scale turbulence generated by the obstacles. The BR also has a strong impact on the amount of flow momentum lost as the flow passes over the obstacle configuration. Both obstacle configurations C2 and C3 have similar velocity traces in the initial regions, but C3, the obstacle with a smaller blockage ratio, achieves a considerably higher velocity within the confines of the obstacle configuration, because of the lower momentum losses. Previous studies indicate that as the blockage ratio increases to a critical value, ranging from roughly 0.3 to 0.6, the flame velocity is able to increase further because of greater flame stretching, but beyond the critical value the flame velocity is dramatically reduced.<sup>7,11,12</sup> Although the C-J detonation velocity is achieved at the tube exit in configuration C3, the wave takes longer to develop and reach the C-J deflagration velocity as compared with configuration C4. This is argued to be because of the presence of larger obstacles (BR = 0.41) at the beginning of the tube, which are more effective at producing large-scale turbulence in the initial region where the propellant flow velocities are low.

The wave velocity is observed to roughly asymptote to the C-J deflagration velocity within the obstacle configuration, in obstacle configurations C3 and C4, where the obstacle configuration length is longer than necessary. The measured wave velocity (~1150 m/s) around 0.7 m from the injector surface is slightly higher than the calculated C-J deflagration velocity (1030 m/s), but is within the 8% measured error for the detonation velocity. The duration of propagation at the C-J deflagration velocity can be reduced by roughly half that observed for configuration C3 by shortening the length of the obstacle configuration. When the obstacle configuration length is shortened to terminate as soon as the C-J deflagration velocity is attained, the time spent at the C-J deflagration velocity is dramatically reduced as demonstrated in configuration C5. Reaching the C-J deflagration velocity within the obstacle configuration appears to be a necessary condition for transition to detonation to occur after the

wave leaves the obstacle configuration as suggested by Ciccarelli and Boccio.<sup>26</sup> After the flame achieves the C-J deflagration velocity and leaves the obstacle configuration, it continuously accelerates until it achieves the C-J detonation velocity. If the obstacle configuration is terminated prematurely, as in configuration C7, the wave does not achieve the C-J deflagration velocity before leaving the obstacle configuration, and consequently it fails to transition to detonation. Structural supports were added to the obstacle configuration at the 1.2-m location to keep the obstacle rods flush to the tube walls and out of the window viewing area. This structural support is responsible for the detonation decelerating at approximately 1.3 m from the closed end, as seen in the C8 trace. The detonation then reaccelerates downstream as a result of reinitiating mechanisms.<sup>26</sup> Configuration C8 allowed the wave to attain C-J detonation velocity in the shortest distance, and it was used in subsequent imaging studies.

The flame and compression wave speeds as measured in the laboratory frame of reference for obstacle configuration C8 are shown in Fig. 5 as a function of the distance along the tube ( $x$ ). Several interesting observations regarding the velocity profiles can be made. In the early stage of flame acceleration ( $x < 0.2$  m), the compression waves travel at the local acoustic speed ( $\sim 300$  m/s), and move away from the low-velocity deflagration. Before reaching the C-J deflagration velocity (1030 m/s), the train of compression waves in front of the reaction zone begin to coalesce into a normal shock.

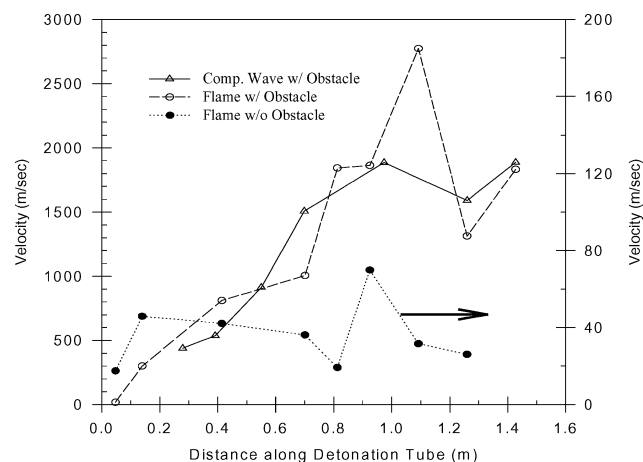


**Fig. 5** Flame and compression wave speeds with the obstacle configuration present and the flame speed without the obstacle configuration present.

As the waves propagate down the tube, they raise the temperature and pressure of the reactants based on simple shock relationships ( $0.2 \text{ m} < x < 0.5 \text{ m}$ ). This increase in temperature and pressure, and possibly along with obstacle-induced flame stretching, allow the flame to accelerate to a slightly higher velocity than the compression waves and decreases the separation between the two. As the flame continues downstream ( $0.5 \text{ m} < x < 1 \text{ m}$ ), the close proximity of the reaction zone and compression wave enables further strengthening of the leading shock wave. In the last stages of the DDT process, localized explosions occur in the region behind the leading shock wave, which accelerates the wave to the point where autoignition occurs immediately behind it. This phenomenon first observed by Urtiew and Oppenheim<sup>17</sup> is ultimately responsible for the onset of the detonation wave.<sup>28</sup> Autoignition initiates a reaction zone close behind the shock wave ( $1 \text{ m} < x < 1.2 \text{ m}$ ), which makes the reaction zone velocity appear to greatly exceed the C-J detonation velocity as seen in Fig. 5. This is similar to observations in the hydrogen-air mixture detonation study performed by Ciccarelli and Boccio.<sup>26</sup> Sileem et al.<sup>18</sup> predicted the flame speed to be higher than the wave speed during the rapid transition period when the accelerating flame and the newly ignited region (autoignition) that begins behind the shock momentarily generate a huge amount of chemical energy, leading to the “explosion.” After autoignition occurs, the flame and shock propagates at the same velocity and remains closely coupled ( $x > 1.2 \text{ m}$ ).

A flame velocity profile with no obstacle configuration in the tube is plotted along the right-hand axis in Fig. 5 to demonstrate the dramatic effect of the obstacle configuration on the flow. Without an obstacle configuration, the combustion-generated expansion of the products is too weak to produce a meaningful compression wave. As expected, the flame velocity is one to two orders of magnitude lower than that of a combustion wave with the obstacle in the tube. Again, it is emphasized that the obstacle configuration dramatically impacts the combustion characteristics of the DDT process.

#### Flame Acceleration Without Obstacle Configuration

Visualization of a flame propagating in the tube without the obstacle configuration was acquired to compare with the images presented in the following sections and improve understanding of the role of the obstacle in flame acceleration and transition to detonation. Schlieren and OH-PLIF images of the deflagration without an obstacle configuration are shown in Figs. 6 and 7 for two axial locations. The times shown in these figures are from the time of ignition. All of the features that are present in the schlieren images are caused by combustion phenomena, where the flame speeds in these images are  $\sim 40$  m/s with respect to the laboratory frame of reference.

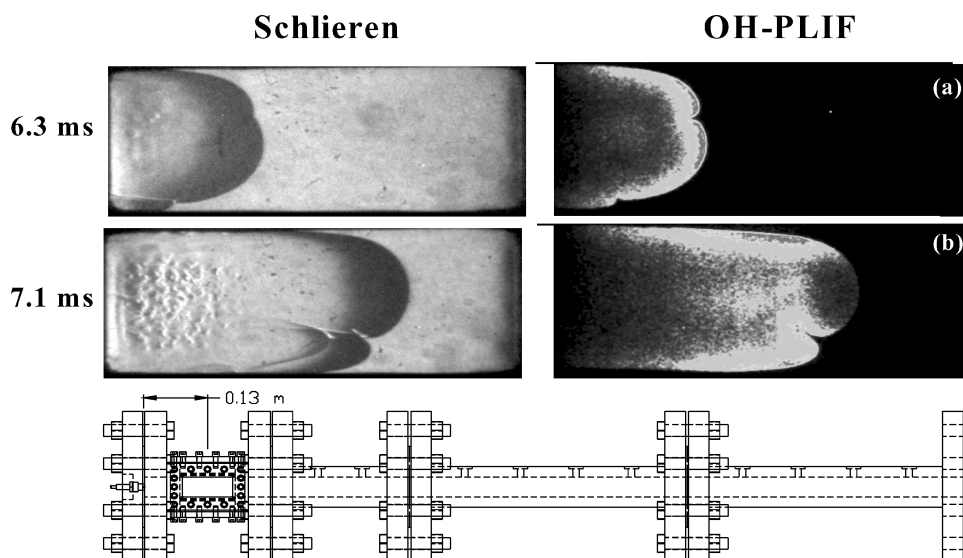


**Fig. 6** Images of flame acceleration without the obstacle configuration present, 0.13 m from closed end: light and dark shading indicate high and low signal intensity, respectively. Flow is from left to right.

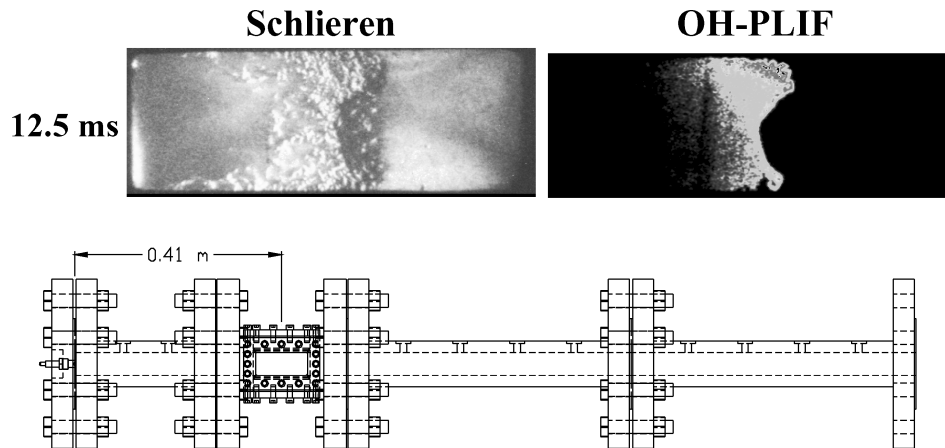


**Fig. 7** Images of flame acceleration without the obstacle configuration present, 0.41 m from closed end: light and dark shading indicate high and low signal intensity, respectively. Flow is from left to right.

Images taken with the window section centered 0.13 m from the closed end are shown in Fig. 6. The two image pairs were taken 0.8 ms apart and illustrate the flame beginning to transition from laminar to turbulent behavior. The increase in volume of the hot combustion products drives the reactants ahead of the flame front at a low initial velocity on the order of the flame speed, allowing the nearly laminar flame structure observed here. The combustion is localized to a thin sheet that slowly propagates down the tube. Local flame-front speeds estimated from OH images are approximately 42 and 19 m/s at the tube centerline and near the wall, respectively. A few large-scale folds in the flame front can be observed in both image pairs, but they are especially obvious in the schlieren (b) image. These wrinkles arise from shear produced between the reactant flow and the wall of the tube. The flame wrinkling tends to weaken the local reaction rate, but the net effect is an increase in burning rate caused by an overall increase in flame-front area. Some enhancement in the burning rate can also be observed near the walls in OH-PLIF (a), which is likely caused by the shear produced in the flow boundary layer stretching the flame surface.

The flame acceleration further downstream is shown in Fig. 7 for the window section centered 0.41 m from the closed end. The flame front is now fully turbulent. The small-scale turbulence induced in the boundary layer along the walls helps to intensify combustion and allows the flame to propagate more rapidly there. The indentation in the flame front at the tube centerline is likely enhanced by a fluid instability, that is perturbed by compression waves reflecting from the tube closed end and side walls. The flow and consequently the flame would remain turbulent because of a continual input of energy from the boundary layer near the wall.

#### DDT Process Analysis

A series of simultaneous schlieren and OH-PLIF images were taken at different regions in the detonation tube for obstacle configuration C8 to closely examine the role that the obstacles play in accelerating DDT.

#### Initial Flame Acceleration

Simultaneous schlieren and OH-PLIF images obtained at different times with the window section centered 0.13 m from the closed end are shown in Fig. 8 in which the first three obstacles have a blockage ratio of 0.41, whereas the last two obstacles have a blockage ratio of 0.28. The times associated with each image pair are based on an arbitrary zero time. Although each pair of images was taken during a separate experiment, experiments performed with identical timing demonstrated excellent repeatability. Figure 8 shows a rapid flame acceleration region, where the measured flame velocity increased from  $\sim 15$  m/s at the start of the window section to nearly 300 m/s at the end of window section. This behavior is in agreement with the exponential acceleration predicted for repeated obstacles in previous theoretical work.<sup>10,28</sup> The velocities are low in this region, and so compression waves generated by the dilating hot product

gases will be acoustic waves that rapidly propagate away from the flame. All of the features that are visible in the schlieren images are caused by combustion phenomena.

In the first image pair, the combustion occurs along the large-scale vortex that is formed by the flow passing the second obstacle [schlieren (a)], but no combustion is evident on the tube centerline after the second obstacle [OH-PLIF (a)]. Here, it is worth noting the evolution of the flame front in terms of the changes in the length scales as the flame proceeds through the obstacle section [see OH-PLIF (a-e)]. The leading edge of the flame front is smooth and nearly laminar [schlieren (a)]. Combustion is distributed across the tube just before the second obstacle [OH-PLIF (a)]. Even after the flame has propagated further downstream [OH-PLIF (b)], there is still no significant combustion in the center of the region after the second obstacle, indicating that the flame is contained within the vortex shed by the obstacle, which takes time to propagate to the tube centerline. This observation supports the claim of Moen and coworkers<sup>10,11</sup> that the initial obstacle-induced flame acceleration is dominated by the large-scale vortical structures that dramatically distort the flame surface and consequently increase the burning rate.

In the third image pair, the influence of small-scale turbulence becomes more apparent. The cascading of the large-scale turbulence behind the second obstacle into smaller scales is apparent in comparing the leading edge of the flame front in schlieren (a) and schlieren (c). These finer scales of turbulence dramatically increase the flame burning surface, allowing rapid propagation of combustion across the region in front of the third obstacle [schlieren and OH-PLIF (c)]. There is also a pronounced effect of small-scale turbulence in the boundary layer, which allows the reaction zone to rapidly propagate along the top wall of the tube between obstacles three and four [OH-PLIF (c)].

The large-scale eddies still dominate the behavior as the flame propagates around the third obstacle in schlieren plate (d), but the turbulent wrinkling of the flame dramatically increases the rate at which the large eddy burns out, and combustion sweeps across the area in front of the fourth obstacle and into the region behind the fifth obstacle [schlieren and OH-PLIF plate (e)]. There is also some confined heat release in the stagnation region in front of the fourth obstacle [OH-PLIF (e)].

The images shown in Fig. 8 are in excellent agreement with the conclusions of Moen et al.<sup>10</sup> in that the initial acceleration of flames by repeated obstacles is dominated by large-scale eddies. However, as the large-scale eddies cascade into smaller-scale turbulence, the smaller-scale eddies serve to increase the transport of heat and mass across the flame front and further increase the burning rate, by more rapidly burning out the large-scale eddies.

#### Shock-Wave Formation

The increase in volume of the combustion products produces a train of weak compression waves that propagate into the reactants ahead of the flame. As the flame accelerates, the product temperature

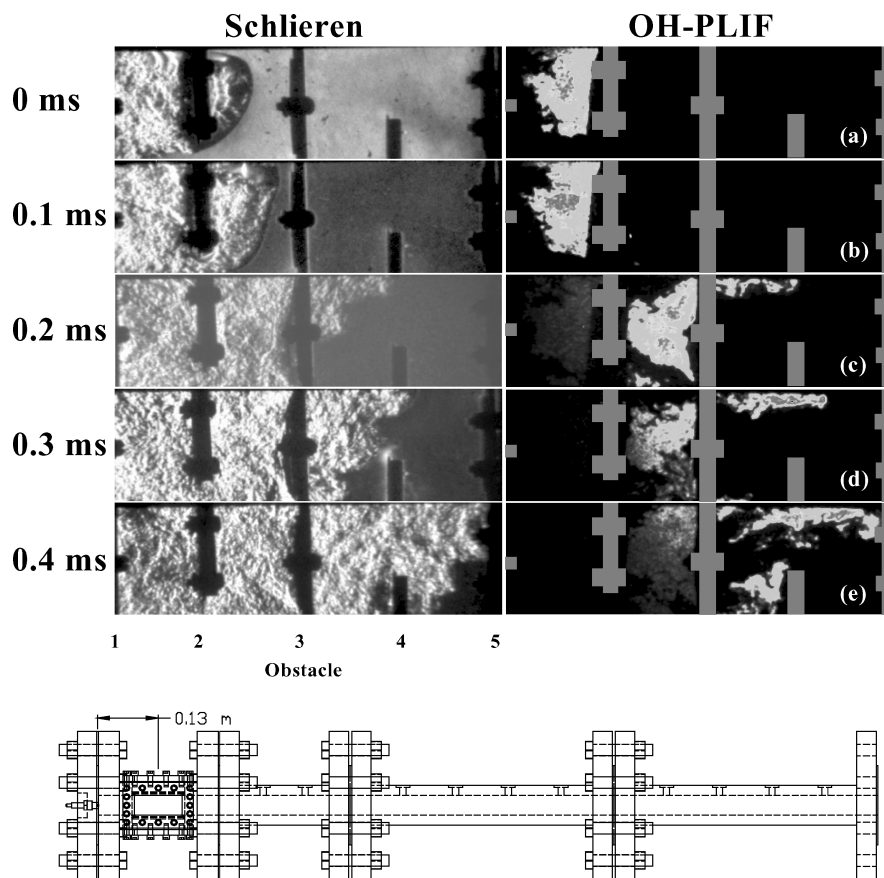


Fig. 8 Images in the initial flame acceleration region, 0.13 m from closed end: light and dark shading indicate high and low signal intensity, respectively. Flow is from left to right.

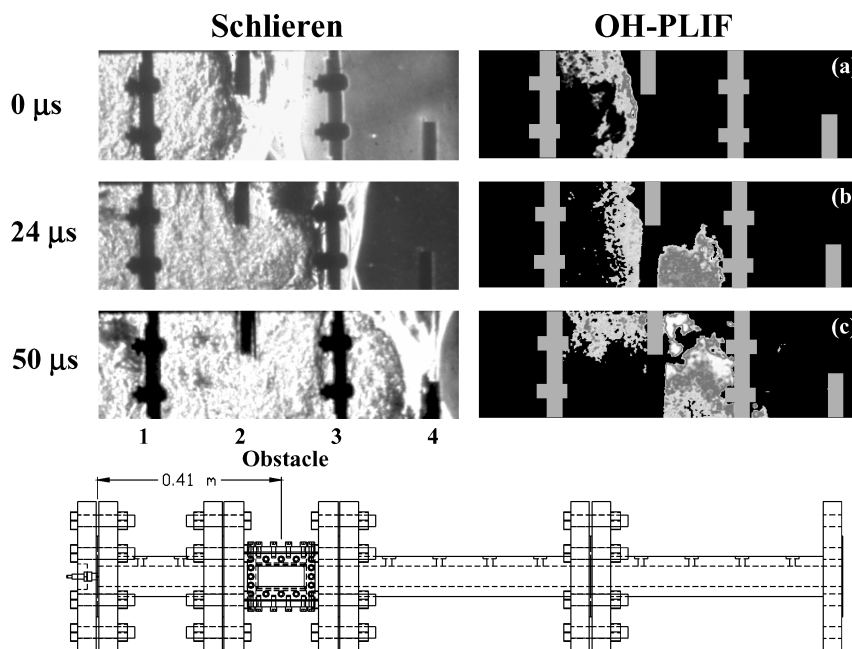
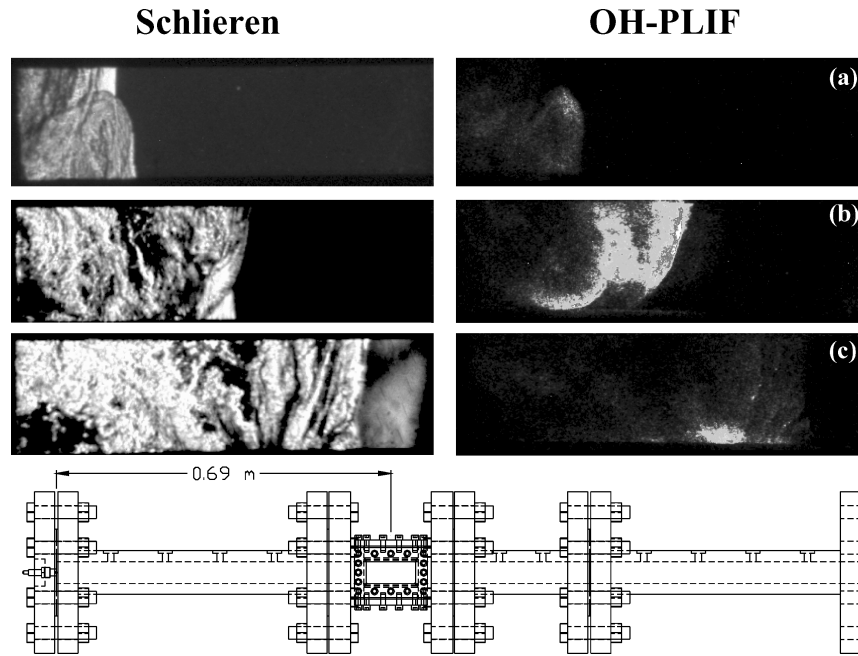


Fig. 9 Images in the shock-wave formation region, 0.41 m from closed end: light and dark shading indicate high and low signal intensity, respectively. Flow is from left to right.

increases, and the compression waves can coalesce into a shock wave. During this process, the role of the obstacle is to continue to increase the flame surface area by generating large-scale turbulence and to provide surfaces for the compression waves to reflect from and redirect them back toward the flame front. The passage of the compression waves directly increases the temperature and pressure of the reactants, which increases the burning rate. The compression waves also tend to destabilize the interface between the cold

reactants and hot products, producing a fluid instability.<sup>28</sup> This instability provides additional deformation of the flame front, which also serves to increase the flame burning rate.

The schlieren and OH-PLIF images obtained with the window section centered 0.41 m from the closed end are depicted in Fig. 9. The times associated with each image pair are based on an arbitrary zero time. Accumulations of strong compression waves are clearly observed in all of these images as the farthest right flow feature in



**Fig. 10** Images in the region of explosion center formation, 0.69 m from closed end: light and dark shading indicate high and low signal intensity, respectively. Flow is from left to right.

the schlieren images. The compression wave velocity in this region increases from  $\sim 500$  to  $\sim 800$  m/s. The heat release shown in these OH-PLIF images is intense and broadly distributed. The reaction zone shown in the figure consists of the apparently defined reaction zone and the volumetric reaction zone. As can be seen from the eddy developed around the second obstacle in OH-PLIF (a) and (b), the large-scale turbulence generated by the obstacles is still a predominant feature of the flow. The flow is highly turbulent at this point, and the fine-scale turbulence helps to rapidly burn out the large-scale eddies, as seen in OH-PLIF (c).

The obstacles also affect the coupling between the compression waves and the reaction zone. The compression waves can freely move downstream into the open region between the second and third obstacles [schlieren (a)]. In plate (b), the wave speed has been retarded near the third obstacle, which allows the combustion to approach and further strengthen the compression waves. In the region after the third obstacle, the compression waves are once again able to move away from the reaction zone. The turbulent flow around the obstacles produces a highly three-dimensional distribution in the reaction zone and leaves some pockets of reactants, such as the wake of the second obstacle, where combustion is delayed [plate (b)]. When the mixture trapped in the wake of the second obstacle starts to react, the compression waves have already propagated well downstream [plate (c)].

The approximate separation lengths between the flame front and precursor shock wave are calculated from the images. The separation length is the axial distance from the flame front to the compression wave front, which directly indicates the strength of the coupling between the two waves. Along the tube centerline, the separation length decreases from approximately 16 to 7 mm when the flame occurs at the middle of the image. However, the length starts to increase to approximately 26 mm again as the flame travels further downstream. Such oscillation in the wave coupling continues as the waves propagate down the tube, but continues to decrease in amplitude until the onset of detonation. It is also emphasized that the flowfield is highly three dimensional because of the interaction of the flow with the obstacles.

#### Explosion Center Formation

With the window section centered 0.69 m from the igniter, the intense chemical reactions present during this stage of the DDT dramatically reduce the signal-to-noise ratio of the OH-PLIF measurements. Because of this difficulty, flame chemiluminescence

(OH\* emission) is responsible for much of the OH signal strength for images taken in this region.

A series of images of the flame evolution, taken with the window section centered 0.69 m from the closed end are shown in Fig. 10. The left edge of the field of view is 0.11 m from the end of the obstacle configuration. The compression wave speed measured in this section increases from  $\sim 1200$  to  $\sim 1500$  m/s, higher than both the C-J deflagration velocity and the flame speed. The compression waves are closely coupled to the turbulent flame brush that follows the wave front [schlieren and OH-PLIF (a) and (b)]. There are no longer obstacles in the flow path to directly generate large-scale eddies in the flow, but the reflection of compression waves from the tube walls and from the tube closed end tends to enable the same fluid instability that was discussed in the previous region. This interaction between the compression waves and the interface between the product and reactant gases deforms the flame front and tends to increase the surface area.

The compression wave front in schlieren (a) is highly convoluted and corrugated, and some of this corrugation persists in schlieren (b), even though the wave front has become more normal. This strong variation in compression wave structure and intensity is reflected in the distribution of heat release across the tube, which closely follows the structure of the compression wave front [OH-PLIF (a) and (b)]. This correspondence in the compression wave and heat-release structure is indicative of coherent energy release, which serves to amplify and strengthen the compression wave front and then further strengthens the reaction zone intensity. This behavior is essential to transition to detonation and is part of an acceleration mechanism proposed by Lee and Moen known as SWACER or shock-wave amplification through coherent energy release.<sup>28</sup> This coupling of the heat release with the compression wave allows for their rapid amplification, which is essential for achieving transition to detonation.

The final process that leads to transition to detonation is the occurrence of localized explosions in trapped pockets of unburned reactants. These explosions send out blast waves, which are amplified by the aforementioned coherent energy release and serve to drive the compression wave front past the C-J detonation velocity and allow the formation of a self-sustained detonation. An intense localized explosion is seen in the flow boundary layer in plate (c) of Fig. 10.

#### Detonation Formation

A normal detonation wave established in the window section centered 0.97 m from the closed end is shown in Fig. 11. As in the

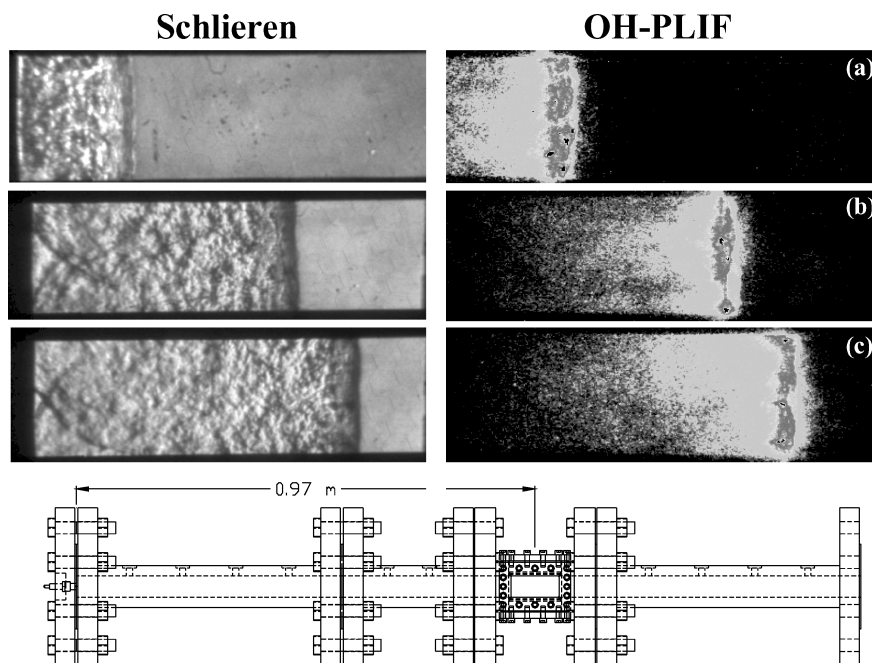


Fig. 11 Images of an established detonation wave, 0.97 m from closed end: light and dark shading indicate high and low signal intensity, respectively. Flow is from left to right.

preceding subsection, the flame chemiluminescence is very intense and is responsible for much of the OH signal in the images presented. At this point, the compression waves that were observed in the previous region have fully coalesced into a strong normal shock. The shock is strong enough to cause autoignition in the reactants, and it is closely followed by a nearly uniform and very intense reaction zone. Transverse waves can be seen on the left-hand side of schlieren (b) and (c), well behind the reaction zone. These waves play an important role in establishing the true three-dimensional structure of the detonation wave.

The maximum steady flame velocity achieved without an obstacle configuration was  $\sim 40$  m/s, one to two orders of magnitude less than the C-J detonation velocity. This reemphasizes the important role that the obstacle configuration plays in accelerating the DDT process. In particular, the large-scale turbulence that is produced as the propellant flow interacts with the obstacles, and the smaller turbulence that those large-scale eddies cascade into, dramatically accelerate the burning rate. This rapid increase in burning rate allows the rapid generation of compression waves, which precondition the reactants and further accelerate the combustion process. The fundamental step of the DDT process is the successful production of a shock wave strong enough to autoignite the reactants. If the burning rate rises rapidly, the compression wave energy will be more compactly distributed along the length of the tube, and the coupling of reaction zone and shock wave will be much stronger. The obstacle configuration C8 used in this study had the additional benefit of reflecting compression waves back toward the reaction front, which served to increase the reaction rate and keep the compression waves from propagating down the tube and decoupling themselves from the reaction zone.

#### Multicycle Results

Multicycle results with the square detonation tube were obtained for 10-Hz operation using ethylene and air, but further increases in repetition rate were hindered by problems with filling the tube completely and igniting the rapidly moving mean flow. The C8 obstacle configuration as shown in Fig. 3 was used for the multicycle experiments. A 50% reduction in DDT time from 6 to 3 ms was observed when compared to the single-shot experiments, but the DDT length remained unaffected around 0.95 m.

Compression wave velocities from several detonations in one multicycle experiment are shown in Fig. 12. In addition, a com-

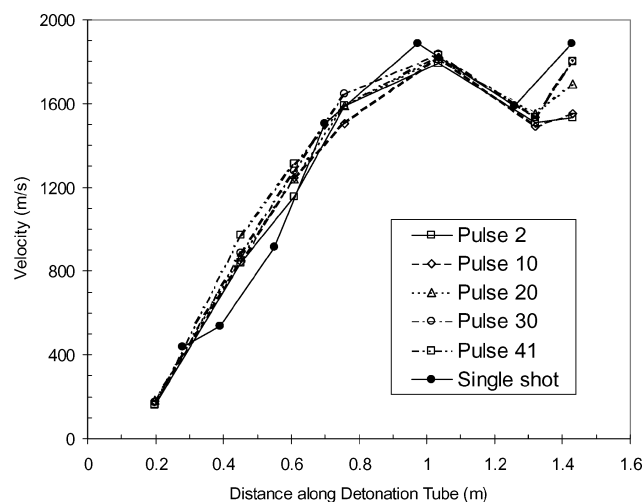
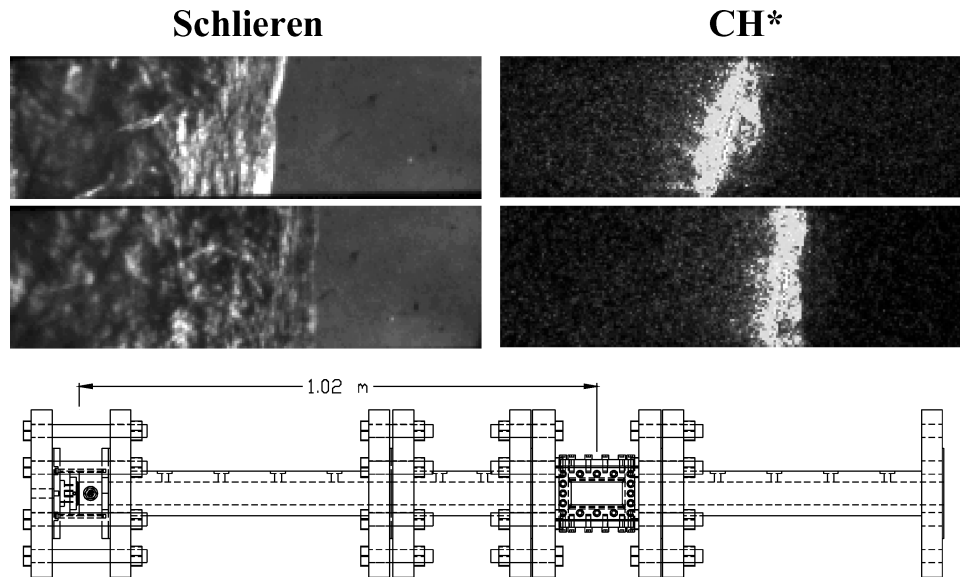


Fig. 12 Compression wave velocities for multicycle operation from the closed end.

pression wave velocity trace from a typical single-shot experiment using the same obstacle as shown in Fig. 4 is also shown in the figure for comparison. The decrease in velocity in Fig. 12 at approximately 1.2 m from the injector face is caused by the detonation being perturbed by a structural support used to keep the obstacle rods flush to the walls in the imaging section. The multicycle detonations were very consistent from shot to shot, with the only observable change being at the last position, where the velocity slightly increases as the detonation tube temperature increases. The influence of dynamic injection on DDT is clearly observed in the initial portion of the tube, where the multicycle detonations accelerate much faster than for the corresponding quiescent single-shot case because of the existence of mean flow velocity and turbulence at the time of ignition.

Simultaneous  $\text{CH}^*$  chemiluminescence and schlieren images were acquired during multicycle operation at a rate of 5 Hz, during 10-Hz operation. Note that  $\text{CH}^*$  chemiluminescence provides the flame emission, which is similar to  $\text{OH}^*$  chemiluminescence. Two pairs of typical images are shown in Fig. 13, taken 1.02 m from the injector face. These results are very similar to those obtained in single-shot operation at the similar location (Fig. 11).



**Fig. 13** Multicycle images of transition to detonation region: light and dark shading indicate high and low signal intensity, respectively. Flow is from left to right. These images were obtained using the signal from the pressure transducer 0.7 m from the injector face to trigger the laser. The time that elapsed from the instant that the laser was triggered to the acquisition of the image was approximately 385  $\mu$ s. The imaging rate was 5 Hz for multicycle operating conditions of 10 Hz.

### Conclusions

The DDT-enhancing characteristics of helically configured flat-plate obstacle were examined systematically in a series of single-shot ethylene-air experiments. The large-scale turbulence generated by the flow interaction with the obstacles was shown to dramatically increase the flame surface area and consequently increase the burning rate. The production of fine-scale turbulence in the flow boundary layer and in the breakdown of the large-scale vortices was also observed to increase the local burning rate and dramatically accelerate the burning velocity. Obstacle blockage ratios between 0.3 and 0.6 and sufficient obstacle spacing were found to provide optimum levels of flame stretching without inducing excessive flow drag.

For all obstacle configurations, the critical step to achieving detonation in these experiments was attaining the C-J deflagration velocity within the obstacle configurations. Any length of obstacle after the compression waves reached the C-J deflagration velocity was observed to be unnecessary and delayed the onset of detonation. After attaining the C-J deflagration velocity, the flame would remain at that speed until it reached the exit of the obstacle configuration, where it would proceed to accelerate and transition to detonation. If the wave had not reached the C-J deflagration velocity before exiting the tube, the compression waves and reaction would decouple, and DDT would not occur.

In the imaging study of the obstacle configuration C8, the reaction rate was also accelerated by the action of compression waves that emanated from the expanding hot product gases. Reflection of the compression waves back toward the flame surface also served to excite a fluid instability that further stretched the flame surface and increased the burning rate. The obstacles used in these experiments enhanced this process by providing numerous surfaces to reflect the compression waves back toward the flame front. The obstacle configuration also hindered the progress of the compression waves in propagating down the tube until the burning rate was fast enough to maintain coupling between the flame front and the compression waves. Once the shock wave was sufficiently strong, autoignition occurred, and a closely coupled reaction zone was established behind the shock, thus forming a self-sustained detonation wave.

Multicycle experiments were also conducted in the square tube to examine the effect on the DDT process of the initial mean flow and turbulence resulting from dynamic injection of the propellants into the tube. Repeatable operation at 10 Hz showed a decrease in DDT time from 6 to 3 ms, whereas the DDT length remained

constant around 0.95 m. Multicycle images of the transition from a fast deflagration to a normal detonation wave were found to be very similar to the results obtained for the single-shot experiments.

### Acknowledgments

The authors gratefully acknowledge funding from the Office of Naval Research under Grant N00014-99-1-0744 with Gabriel D. Roy serving as contract monitor. The authors also thank the reviewers for their extensive comments and constructive criticism. Their input helped to significantly enhance this paper in terms of its clarity and precision of terminology.

### References

- Bratkovich, T., and Bussing, T., "A Pulse Detonation Engine Performance Model," AIAA Paper 95-3155, July 1995.
- Eidelman, S., Grossman, W., and Lottati, I., "Review of Propulsion Applications and Numerical Simulations of the Pulsed Detonation Engine Concept," *Journal of Power and Propulsion*, Vol. 7, No. 6, 1991, pp. 857–865.
- Zitoun, R., and Desbordes, D., "Propulsive Performance of Pulsed Detonations," *Combustion Science and Technology*, Vol. 144, Nos. 1–6, 1999, pp. 93–114.
- Kailasanath, K., "Review of Propulsion Applications of Detonation Waves," *AIAA Journal*, Vol. 38, No. 9, 2000, pp. 1698–1708.
- Mattison, D., Brophy, C., Sanders, S., Ma, L., Hinckley, K., Jeffries, J., and Hanson, R., "Pulse Detonation Engine Characterization and Control Using Tunable Diode-Laser Sensors," *Journal of Power and Propulsion*, Vol. 19, No. 4, 2003, pp. 568–572.
- Lindstedt, R., and Michels, H., "Deflagration to Detonation Transitions and Strong Deflagrations in Alkane and Alkene Air Mixtures," *Combustion and Flame*, Vol. 76, No. 2, 1989, pp. 169–181.
- Moen, I., Lee, J. H. S., Hjertager, B., Fuhre, K., and Eckhoff, R., "Pressure Development due to Turbulent Flame Propagation in Large-Scale Methane-Air Explosions," *Combustion and Flame*, Vol. 47, No. 1, 1982, pp. 31–52.
- Hjertager, B., Fuhre, K., Parker, S., and Bakke, J., "Flame Acceleration of Propane-Air in a Large-Scale Obstructed Tube," *Dynamics of Shock Waves, Explosions, and Detonations*, edited by J. R. Bowen, N. Manson, A. K. Oppenheim, and R. I. Soloukhin, Vol. 94, Progress in Astronautics and Aeronautics, AIAA, New York, 1984, pp. 504–522.
- Lindstedt, R., and Michels, H., "Deflagration to Detonation Transitions in Mixtures of Alkane LNG/LPG Constituents with  $O_2/N_2$ ," *Combustion and Flame*, Vol. 72, No. 1, 1988, pp. 63–72.
- Moen, I., Donato, M., Knystautas, R., Lee, J. H. S., and Wagner, H., "Turbulent Flame Propagation and Acceleration in the Presence of Obstacles," *Gasdynamics of Detonations and Explosions*, edited by J. R. Bowen, N. Manson, A. K. Oppenheim, and R. I. Soloukhin, Vol. 75, Progress in Astronautics and Aeronautics, AIAA, New York, 1981, pp. 33–47.

<sup>11</sup>Moen, I., Donato, M., Knystautas, R., and Lee, J. H. S., "Flame Acceleration due to Turbulence Produced by Obstacles," *Combustion and Flame*, Vol. 39, No. 1, 1980, pp. 21–32.

<sup>12</sup>Chan, C., Moen, I., and Lee, J. H. S., "Influence of Confinement on Flame Acceleration due to Repeated Obstacles," *Combustion and Flame*, Vol. 49, No. 1, 1983, pp. 27–39.

<sup>13</sup>Benedick, W., Guirao, C., Knystautas, R., and Lee, J. H. S., "Critical Charge for the Direct Initiation of Detonation in Gaseous Fuel/Air Mixtures," *Dynamics of Explosions*, edited by J. R. Bowen, J.-C. Leyer, and R. I. Soloukhin, Vol. 106, Progress in Astronautics and Aeronautics, AIAA, New York, 1986, pp. 181–202.

<sup>14</sup>Kiyanda, C. B., Tanguay, V., Higgins, A. J., and Lee, J. H. S., "Effect of Transient Gasdynamic Processes on the Impulse of Pulse Detonation Engines," *Journal of Propulsion and Power*, Vol. 18, No. 5, 2002, pp. 1124–1126.

<sup>15</sup>Cooper, M., Jackson, S., Austin, J., Wintenberger, E., and Shepherd, J. E., "Direct Experimental Impulse Measurements for Detonations and Deflagrations," *Journal of Propulsion and Power*, Vol. 18, No. 5, 2002, pp. 1033–1041.

<sup>16</sup>Guirao, C., Knystautas, R., and Lee, J. H. S., "A Summary of Hydrogen-Air Detonation Experiments," NUREG/CR-4961 (SAND 87-7128), U.S. Nuclear Regulatory Commission, Washington, DC, 1987.

<sup>17</sup>Urtiew, P., and Oppenheim, A., "Experimental Observations of the Transition to Detonation in an Explosive Gas," *Proceedings of the Royal Society of London, Series A*, Vol. 295, No. 1440, 1966, pp. 13–28.

<sup>18</sup>Sileem, A., Kassoy, D., and Hayashi, A., "Thermally Initiated Detonation Through Deflagration to Detonation Transition," *Proceedings of the Royal Society of London, Series A*, Vol. 435, No. 1895, 1991, pp. 459–482.

<sup>19</sup>Chan, C., "Collision of a Shock Wave with Obstacles in a Combustible Mixture," *Combustion and Flame*, Vol. 100, Nos. 1–2, 1995, pp. 341–348.

<sup>20</sup>Dorofeev, S. B., Sidorov, V. P., Dvoishnikov, A. E., and Breitung, W., "Deflagration to Detonation Transition in Large Confined Volume of Lean Hydrogen-Air Mixtures," *Combustion and Flame*, Vol. 104, Nos. 1–2, 1996, pp. 95–110.

<sup>21</sup>Eder, A., and Brehm, N., "Analytical and Experimental Insights into Fast Deflagrations, Detonations, and the Deflagration-to-Detonation Transition Process," *Heat and Mass Transfer*, Vol. 37, No. 6, 2001, pp. 543–548.

<sup>22</sup>Santoro, R., Broda, J., Conrad, C., Woodward, R., Pal, S., and Lee, S.-Y., "Multidisciplinary Study of Pulse Detonation Engine Propulsion," *JANNAF*, CPIA Publication 692, Vol. 1, 1999, pp. 141–150.

<sup>23</sup>Knystautas, R., Guirao, C., Lee, J. H. S., and Sulmistras, A., "Measurements of Cell Size in Hydrocarbon-Air Mixtures and Predictions of Critical Tube Diameter, Critical Initiation Energy, and Detonability Limits," *Dynamic of Shock Waves, Explosions, and Detonations*, edited by J. R. Bowen, N. Manson, A. K. Oppenheim, and R. I. Soloukhin, Vol. 94, Progress in Astronautics and Aeronautics, AIAA, New York, 1984, pp. 23–37.

<sup>24</sup>McBride, B., and Gordon, S., "Computer Program for Calculation of Complex Chemical Equilibrium Compositions and Applications," NASA RP 1311, June 1996.

<sup>25</sup>Knystautas, R., Lee, J. H. S., Shepherd, J., and Teodorczyk, A., "Flame Acceleration and Transition to Detonation in Benzene-Air Mixtures," *Combustion and Flame*, Vol. 115, No. 2, 1998, pp. 424–436.

<sup>26</sup>Ciccarelli, G., and Boccio, J., "Detonation Wave Propagation Through a Single Orifice Plate in a Circular Tube," *Proceedings of the Combustion Institute*, Vol. 27, 1998, pp. 2233–2239.

<sup>27</sup>Chue, R. S., Clarke, J. F., and Lee, J. H. S., "Chapman-Jouguet Deflagrations," *Proceedings of the Royal Society of London, Series A*, Vol. 441, No. 1913, 1993, pp. 607–623.

<sup>28</sup>Lee, J. H. S., and Moen, I., "The Mechanism of Transition From Deflagration to Detonation in Vapor Cloud Explosions," *Progress in Energy and Combustion Science*, Vol. 6, No. 4, 1980, pp. 359–389.

# Elements of Spacecraft Design

Charles D. Brown, Wren Software, Inc.

This new book is drawn from the author's years of experience in spacecraft design culminating in his leadership of the Magellan Venus orbiter spacecraft design from concept through launch. The book also benefits from his years of teaching spacecraft design at University of Colorado at Boulder and as a popular home study short course.

The book presents a broad view of the complete spacecraft. The objective is to explain the thought and analysis that go into the creation of a spacecraft with a simplicity and with enough worked examples so that the reader can be self taught if necessary. After studying the book, readers should be able to design a spacecraft, to the phase A level, by themselves.

Everyone who works in or around the spacecraft industry should know this much about the entire machine.

## Table of Contents:

- |                      |                           |  |
|----------------------|---------------------------|--|
| ❖ Introduction       | ❖ Power System            | ❖ Appendix A: Acronyms and Abbreviations |
| ❖ System Engineering | ❖ Thermal Control         | ❖ Appendix B: Reference Data             |
| ❖ Orbital Mechanics  | ❖ Command And Data System | ❖ Index                                  |
| ❖ Propulsion         | ❖ Telecommunication       |  |
| ❖ Attitude Control   | ❖ Structures              |  |

AIAA Education Series

2002, 610 pages, Hardback • ISBN: 1-56347-524-3 • List Price: \$111.95 • AIAA Member Price: \$74.95

American Institute of Aeronautics and Astronautics  
Publications Customer Service, P.O. Box 960, Herndon, VA 20172-0960  
Fax: 703/661-1501 • Phone: 800/682-2422 • E-mail: warehouse@aiaa.org  
**Order 24 hours a day at [www.aiaa.org](http://www.aiaa.org)**



American Institute of Aeronautics and Astronautics

02-0547

